Radio interferometric imaging of RS Oph bipolar ejecta for the 2021 nova outburst

A&A 666, L6 (2022)
https://doi.org/10.1051/0004-6361/202244821

Astronomy & Astrophysics

LETTER TO THE EDITOR

Radio interferometric imaging of RS Oph bipolar ejecta for the 2021 nova outburst

U. Munari[1], M. Giroletti[2], B. Marcote[3], T. J. O'Brien[4], P. Veres[5], J. Yang[6], D. R. A. Williams[4], and P. Woudt[7]

[1] INAF Osservatorio Astronomico di Padova, 36012 Asiago, VI, Italy
e-mail: ulisse.munari@inaf.it
[2] INAF Istituto di Radioastronomia, Via Gobetti 101, 40129 Bologna, Italy
[3] Joint Institute for VLBI ERIC, Oude Hoogeveensedijk 4, 7991 PD, Dwingeloo, The Netherlands
[4] Jodrell Bank Centre for Astrophysics, School of Physics and Astronomy, University of Manchester, Manchester M13 9PL, UK
[5] Center for Space Plasma and Aeronomic Research (CSPAR), University of Alabama in Huntsville, Huntsville, AL 35899, USA
[6] Dept. of Space, Earth and Environment, Chalmers University of Technology, Onsala Space Observatory, 43992 Onsala, Sweden
[7] Department of Astronomy University of Cape Town, Private Bag X3, Rondebosch 7701, South Africa

Received 27 August 2022 / Accepted 21 September 2022

ABSTRACT

The recurrent nova and symbiotic binary RS Oph erupted again in August 2021 for its eighth known outburst. We observed RS Oph 34 days after the outburst at 5 GHz with the European VLBI Network (EVN). The radio image is elongated over the east–west direction for a total extension of about 90 mas (or about 240 AU at the *Gaia* DR3 distance $d = 2.68^{+0.17}_{-0.15}$ kpc), and shows a bright and compact central component coincident with the *Gaia* astrometric position, and two lobes east and west of it, expanding perpendicular to the orbital plane. By comparing with the evolution of emission-line profiles on optical spectra, we found the leading edge of the lobes to be expanding at ∼7550 km s^{-1}, and $i = 54°$ as the orbital inclination of the binary. The 2021 radio structure is remarkably similar to that observed following the 2006 eruption. The obscuring role of the density enhancement on the orbital plane (DEOP) is discussed in connection to the time-dependent visibility of the receding lobe in the background to the DEOP, and the origin of the triple-peaked profiles is traced to the ring structure formed by the nova ejecta impacting the DEOP.

Key words. novae, cataclysmic variables – stars: winds, outflows

1. Introduction

The recurrent nova and symbiotic binary RS Oph underwent a new outburst in August 2021, following previous outbursts recorded in 1898, 1933, 1958, 1967, 1985, and 2006, with a further probable eruption in 1945 that was partly obscured by the seasonal gap (Adamakis et al. 2011). According to Munari & Valisa (2021), the eruption started on ($t_{\rm ini}$) 2021 Aug. 08.50 (±0.01) UT and the passage through maximum optical brightness ($t_{\rm max}$) occurred on 2021 Aug. 09.58 (±0.05) UT; $t_{\rm ini}$ will constitute our reference epoch throughout this paper.

A nova eruption is rather violent, with 10^{-6}–10^{-4} $M_\odot$ of material being expelled at several 10^3 km s^{-1} as a consequence of thermonuclear runaway (TNR) igniting in the accreted and electron-degenerate shell of a white dwarf (WD). The role played by the powerful shocks that develop in the resulting (multi-component) outflow is being increasingly appreciated (e.g., Aydi et al. 2020; Chomiuk et al. 2021a,b), and even more so for novae that erupt within symbiotic binaries (see Munari 2019, for a recent review), in which the pre-existing wind from the red giant (RG) companion is dense and massive enough to provide a decelerating medium for the nova ejecta that slam into it.

The RS Oph outburst of 2021 triggered widespread interest and was followed across the entire electromagnetic spectrum with meticulous observations; so far, only a very small proportion of the information stemming from these observations has been published. Cheung et al. (2022) presented the outburst evolution in γ-rays at energies >0.1 GeV as recorded by *Fermi*-LAT, showing a broad peak (width ∼1 day) centred perfectly on the optical maximum. H.E.S.S. Collaboration (2022) and Acciari et al. (2022) reported the detection of RS Oph at the even higher energies probed by the Cherenkov telescopes, peaking at day +3.5. Dense monitoring of RS Oph in the X-rays was performed by the *Swift* satellite, which was modelled and compared to similarly extensive observations obtained during the 2006 eruption by Page et al. (2022). The shock-powered, hard X-rays reached maximum intensity on day +5 and behaved very similarly to those observed during the 2006 event, as did the photometric light curve at optical wavelengths. The supersoft X-ray component emerged between days +20 and +25, when the ejected circumstellar material had become sufficiently diluted to clear the view to the central binary. The spectral evolution has also been a close replica of previous eruptions: at optical wavelengths it was documented at high resolution and daily cadence by Munari & Valisa (2021, 2022), and revealed the initial flash-ionization by the TNR of the RG wind, its recombination following an e-folding time of ∼60 h, and the progressive deceleration of the nova ejecta plowing through the pre-existing RG wind.

Preliminary reports of radio observations made during the 2021 outburst of RS Oph have been issued by Williams et al. (2021), Sokolovsky et al. (2021), Nayana et al. (2021), and

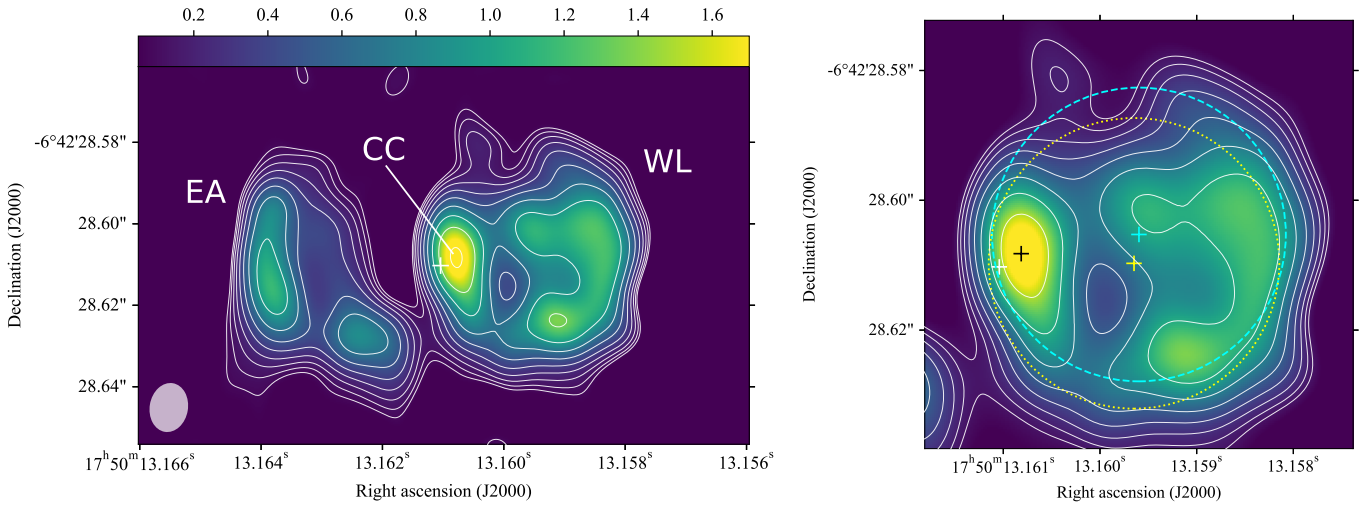

Fig. 1. 5 GHz EVN+*e*-MERLIN image of RS Oph on 2021 Sept. 11, 34.3 days from $t_{\rm ini}$. *Left*: full scale image. The beam size is shown by the ellipse in the bottom left corner (9.4 mas × 12.1 mas in p.a. −8.5°). The white cross represents the position and uncertainty (magnified by a factor of 50 for visibility) of RS Oph in *Gaia* DR3, moved to day +0 by application of proper motions. CC refers to the compact component close to the *Gaia* position, WL to the western round lobe, and EA is the arc structure to the east. The colour scale and contours represent total intensity emission of the cleaned image, starting at $\pm 5\sigma$ (± 0.25 mJy beam^{-1}) and increasing by steps of $\sqrt{2}$. *Right*: zoom onto the WL component, with the best-fit ring and centre from 2021 data overlaid as a cyan dashed line, and the best-fit ring and centre for 2006 from Rupen et al. (2008) shown with the yellow dotted line, ported to the same 2021 epoch by application of *Gaia* DR3 proper motions. The black cross marks the delta component accounting for most of the emission from CC. The colour scale is the same as in the *left panel*, and contours start at 8σ for the sake of clarity.

Peters et al. (2021). These observations explored the frequency range from 0.8 to 35 GHz, started as early as day +2, and recorded an increase in flux with passing days up to the latest observing epoch reported (day +28). They also recorded changes in the spectral index from an initial $\alpha \approx +0.8$ to a later $\alpha \approx -0.3$. The initial inverted spectrum was attributed to external free-free absorption or to synchrotron self-absorption within the radio-emitting region, while the flatter slope and deviations from a simple power law at later epochs (when the absorption was assumed to have mostly cleared) were attributed to inhomogeneities in the emitting region or to partial obscuration by an inhomogeneous absorbing screen. The derived brightness temperatures, ranging from 10^6 K to 10^8 K, indicate a non-thermal origin for the radio emission.

In this Letter we present a European VLBI Network (EVN) radio map of RS Oph from observations made on day +34 at 5 GHz, which is part of a longer monitoring campaign, the details and comprehensive analysis of which will be presented in a dedicated forthcoming publication (Giroletti et al., in prep.).

2. Radio observations

We observed RS Oph with the EVN – including *e*-MERLIN outstations – on 2021 September 11, for 8 h starting at 14.30 UT (day +34.3 at mid run). The observing waveband started at 4.81 GHz, with a bandwidth of 256 MHz, divided into 8 × 32 MHz-wide sub-bands, each recorded in dual-polarisation, for a total data rate of 2 Gbps. The participating telescopes were: Jodrell Bank (Mark2), Westerbork, Effelsberg, Medicina, Shanghai (25 m), Toruń, Hartebeesthoek, Irbene, Yebes, Svetloe, Zelenchukskaya, Badary, and the *e*-MERLIN outstations in Cambridge, Darnhall, Defford, Knockin, and Pickmere. The shortest baseline is Darnhall-Pickmere (16 km, corresponding to 650 mas angular scale), and the longest is Shanghai-Hartebeesthoek (10 161 km, corresponding to 1.0 mas angular scale). Data were electronically transferred to the Joint Institute for VLBI ERIC (JIVE, The Netherlands) and correlated in real time with the SFXC software correlator (Keimpema et al. 2015).

The observations followed a standard phase-referencing scheme, with four-minute scans on RS Oph bracketed by 40-s calibrator scans on the source J1745−0753 at a separation of 1°.67. The initial data reduction was carried out using the latest version of the EVN pipeline based on ParselTongue and AIPS. The calibrated data were then downloaded and inspected with Difmap. Editing, cleaning, and self-calibration were carried out interactively, switching between uniform and natural weights to optimise the contributions of both the short and the long baselines. We also checked the reliability of the self-calibration solutions with task `CALIB` in AIPS, which confirmed smooth variations in phase solutions.

The left panel of Fig. 1 shows the final EVN image. It was obtained in Difmap with natural weights and a Gaussian taper of 0.5 at 10 $M\lambda$, providing a restoring beam of 9.4 mas × 12.1 mas in p.a. −8.5°. The off-source rms noise is 50 μJy beam^{-1}. The total cleaned flux density is 20 mJy, which corresponds to a monochromatic luminosity of 1.7×10^{13} W Hz^{-1}.

3. Discussion

3.1. Radio components

The radio emission of RS Oph in Fig. 1 is elongated over the east–west direction for a total extension of about 90 mas (or about 240 AU at the *Gaia* DR3 distance $d = 2.68^{+0.17}_{-0.15}$ kpc). A compact central component (CC) lies within a few mas of the *Gaia* DR3 position (Gaia Collaboration 2022) extrapolated to the observing epoch. Emission is present on either side of the CC. This emission is brighter on the western side, forming a circular lobe (WL), similarly to what was observed in the 2006 explosion (O'Brien et al. 2006). Fainter emission is present to the east of CC, in the shape of an arc (EA).

Table 1. Results of fitting the delta and ring components as shown in the right panel of Fig. 1.

Component	Type	RA	Dec	Radius	Flux density
CC	Delta	17h50m13.1608s	−06d42′28.6082″	–	0.91 mJy
WL	Ring	17h50m13.1596s	−06d42′28.6053″	22.5 mas	5.6 mJy

Preliminary inspection of the radio images of RS Oph we collected with EVN at other epochs shows that the WL brightens and expands with time. In order to provide a simple yet quantitative representation of the CC and WL, we processed the visibilities with a mixed approach. From the final dataset, we removed all the clean components from CC and those on the outer front of WL, preserving only those in EA and in the inner ∼20 mas of WL. We then carried out an interactive model fitting adding a delta component at the central position and a circular ring on the western residuals. The results of this fit are shown in Table 1. The resulting ring and its centre are shown in cyan overlaid on the clean image in the right panel of Fig. 1.

A similar expanding ring was observed by O'Brien et al. (2006, 2008), Sokoloski et al. (2008), and Rupen et al. (2008) in their VLBI, VLBA, EVN, and MERLIN multi-epoch imaging of RS Oph during the 2006 outburst. On day +26.8 of the 2006 outburst, Rupen et al. (2008) measured the radius of the ring at 5 GHz, finding 17.5(±0.5) mas, and found its centre laying at (J2000) $17^{h}50^{m}13.1583^{s}$, −6°42′28.517″ (±1 mas). In the right panel of Fig. 1, we overplot the centre and ring found by these latter authors in yellow (with its radius linearly increased to match our day +34.3 epoch). The agreement with the 2021 values is remarkable.

3.2. A model for the radio emission of RS Oph

The basic components of our 2021 radio map in Fig. 1 were also present in 2006. The inaccurate ground-based astrometry in 2006 placed RS Oph ∼100 mas away from the radio structure, which did not help in modelling the observations. While a bipolar structure was considered possible by O'Brien et al. (2006), Rupen et al. (2008) interpreted WL as the outer front of the shocked ejecta, expanding in a spherical arrangement away from RS Oph located at the centre, with EA being a polar jet leaving the central binary at a much greater velocity than the spherical ejecta, while CC was considered part of an east–west asymmetry in the brightness distribution of WL.

Thanks to the superb accuracy of the *Gaia* DR3 astrometric position for RS Oph, we are now able to propose a different model for the radio emission of RS Oph that abandons spherical symmetry for the ejecta in favour of a clean bipolar arrangement. The simple sketch in Fig. 2 outlines the basic spatial arrangement of our model and its temporal evolution, for a viewing angle matching the $i \sim 50° \pm 5°$ orbital inclination inferred from orbital solutions of the radial velocity curve of the RG, and the assumed mass of the RG and the WD (Dobrzycka et al. 1996; Fekel et al. 2000; Brandi et al. 2009).

In addition to a massive accretion disk (AD) around the WD, 3D hydrodynamical simulations of symbiotic stars show that much of the mass loss from the RG is gravitationally focused by the companion towards the orbital plane, creating a strong and disk-like density enhancement with the binary at its centre (e.g., Walder et al. 2008; Orlando & Drake 2012; Martin & Dubus 2013; Pan et al. 2015; Booth et al. 2016; Lee et al. 2022). In Fig. 2, the density enhancement on the orbital plane (DEOP) is represented by the diffuse and reddish component.

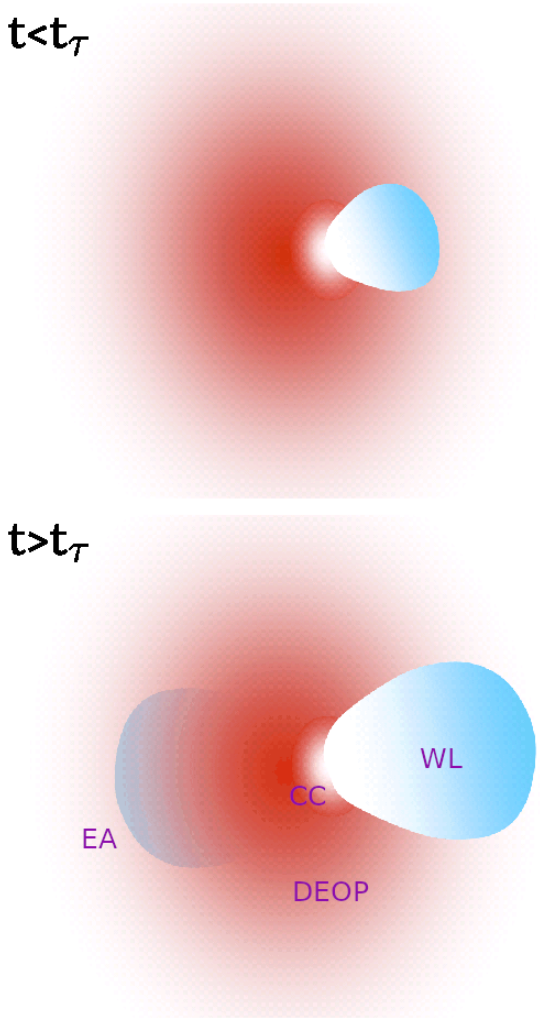

Fig. 2. Simple sketch (not to scale) of the expanding and bipolar arrangement of RS Oph ejecta. The orbital plane is vertical and the viewing angle matches the $i \sim 50° \pm 5°$ inclination inferred from the radial velocity orbit and assumed masses for the RG and WD. For the definition of t_τ (about day +20) and the meaning of the other labels, see Sect. 3.2. The *lower panel* represents the view to RS Oph at the time of the day +34.3 EVN observation, when the leading edge of the receding lobe (EA) has moved past the projected distance from the centre where the free–free opacity of the DEOP in the foreground drops to $\tau_\nu = 1$.

During a nova eruption, the combined effect of the AD and the DEOP is to confine the ejecta primarily within a bipolar structure, which expands perpendicular to the orbital plane. The non-thermal radio emission originates at the shock interface between the fast expanding lobes and the pre-existing slow wind of the RG. The WL component in Fig. 1 is the projection on the plane of the sky of the lobe moving towards us, in the foreground to the DEOP. EA is the visible outer portion of the lobe expanding opposite the WL, moving away from us and located behind the DEOP.

The projected surface density of the DEOP, and probably also its ionisation degree, radially declines moving away from the central binary, which implies that the free-free opacity exerted by the DEOP also reduces as a function of the increasing projected distance from its centre. For its synchrotron radiation (of frequency ν) to be able to reach us, the EA component has to move to a projected distance from the central binary (θ_ν) that is large enough to cross the DEOP where the optical depth turns $\tau_\nu < 1$.

As sketched in Fig. 2, at epochs $t < t_\tau$ (where t_τ designates the time EA needs to expand to θ_ν where $\tau_\nu = 1$), the radio emission from EA is completely absorbed by the DEOP, and its presence therefore goes unrevealed. Observations on days +13.8 by O'Brien et al. (2006) and +20.8 by Rupen et al. (2008) pertain to this phase. Conversely, at later $t > t_\tau$ epochs, the emission from EA becomes visible, first from its leading edge and then from the rest, progressively growing in flux density and angular extension as more and more of EA moves beyond the $\tau_\nu = 1$ position. Epochs +21.5 and +28.7 of O'Brien et al. (2006), +26.8 of Rupen et al. (2008), +49 of O'Brien et al. (2008), and +51 of Sokoloski et al. (2008) trace this emersion of EA into visibility. Ultimately, when the whole of EA has moved past θ_ν, it will appear similar in shape and angular extension to WL, and at equal angular distance from the RS Oph astrometric position, a scenario that appears to be consistent with the day +63 radio image of RS Oph presented by O'Brien et al. (2008).

In connection to the obscuration exerted by the DEOP, it is useful to note that Rupen et al. (2008) computed the free-free opacity at 5 GHz predicted for the fully ionised r^{-2} wind from the RG in RS Oph as a function of the observed projected distance. Assuming a mass-loss rate $\dot{M} = 1 \times 10^{-6}\,M_\odot\,\mathrm{yr}^{-1}$ and a $v_\mathrm{w} = 20\,\mathrm{km\,s^{-1}}$ wind velocity, these latter authors found the $\tau_\nu = 1$ threshold being crossed at a projected ~24 mas (65 AU) distance. A lower (higher) mass-loss rate would shorten (widen) this separation. Although the actual $\dot{M}$ of RG or the density profile and ionisation degree of the DEOP may be different, this value is comparable to the distance from the *Gaia* astrometric position at which the inner edge of EA is located in Fig. 1.

We interpret the CC as the interface between the DEOP and the impacting fast ejecta. Its much higher density turns the DEOP into a decelerating medium that is far more efficient than the diffuse wind of RG: a lot of kinetic energy is transformed within a small volume of space, leading to the bright non-thermal emission spike of Fig. 1.

This proposed spatial arrangement for the radio-emitting regions of RS Oph is broadly consistent with the [OIII] imaging obtained by HST at 155 and 449 days after the 2006 outburst, which has been discussed by Ribeiro et al. (2009). The double-ring structure observed by these latter authors on day +155 has an east-west orientation with a total (peak-to-peak) extent of 360(±30) mas in the plane of the sky, corresponding to a (constant) expansion rate of 1.16(±0.1) mas day^{-1}. Projecting it back to our day +34.3 observing epoch, the corresponding total extension would be ~80 mas.

3.3. Comparison with radial velocities

To gain insight into the space velocity of the ejecta and the viewing angle to the RS Oph system, we turn to the daily high-spectral-resolution monitoring of the 2021 outburst of RS Oph presented by Munari & Valisa (2021, 2022) and use it to derive the radial velocity of the leading edge of the ejecta. At the very beginning of the outburst, the glare of the RG wind ionised by the initial UV flash overwhelmed the emission from the expanding ejecta. Only by approximately day +2 had recombination in the wind proceeded enough to allow a clean view of the expanding ejecta. Figure 3 presents the Hα profile of RS Oph for day +2.3. Very sharp emission and absorption spikes are located close to 0.0 radial velocity on the day +2.3 spectrum: the spike in emission ($FWHM \sim 31\,\mathrm{km\,s^{-1}}$, $\mathrm{RV}_\odot = -6.3 \pm 0.4\,\mathrm{km\,s^{-1}}$) originates from the recombining RG wind, and that in absorption ($FWHM \sim 20\,\mathrm{km\,s^{-1}}$, $\mathrm{RV}_\odot = -64.5 \pm 0.8\,\mathrm{km\,s^{-1}}$) comes from the outer and neutral portion of the RG wind (its velocity matching the sum of the barycentric velocity of RS Oph, $-40\,\mathrm{km\,s^{-1}}$, and a 20–25 km s^{-1} value for the terminal velocity of the RG wind). The fastest feature on the spectrum for day +2.3 in Fig. 3 is the $-4700\,\mathrm{km\,s^{-1}}$ edge of the P-Cyg absorption, tracing the fastest material external to the pseudo-photosphere forming in the expanding, cooling, and recombining ejecta.

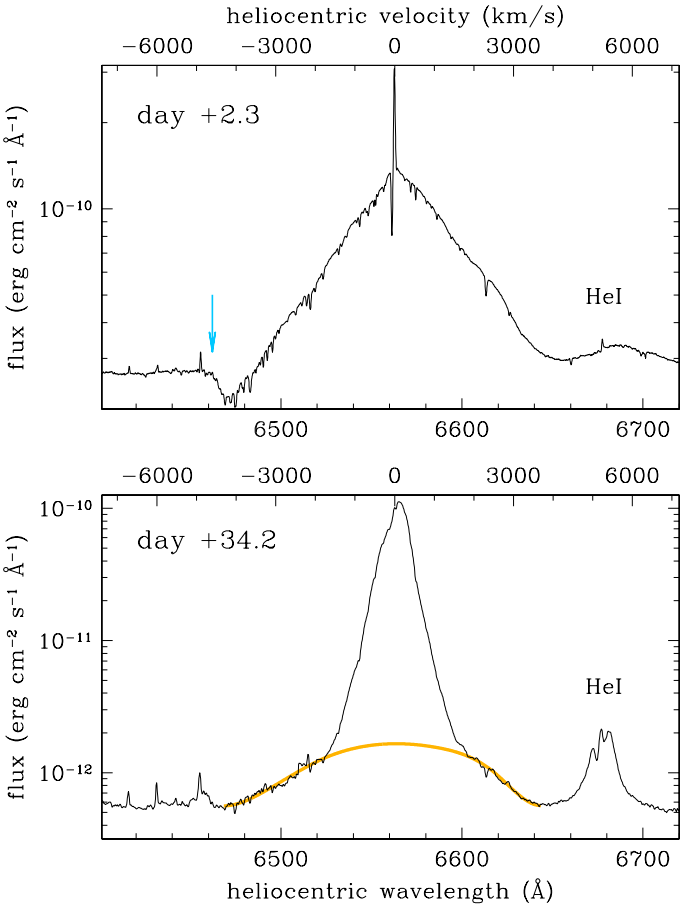

Fig. 3. Sample Hα profiles of RS Oph (from data in Munari & Valisa 2022) early in the outburst and at the time of our EVN radio imaging (see Sect. 3.3 for details). Heliocentric radial velocities are given at the top of the panels. The arrow in the *top panel* marks the $-4700\,\mathrm{km\,s^{-1}}$ terminal velocity of the P-Cyg absorption, while the orange line in the *lower panel* is a fit to the broad pedestal extending up to $-4200\,\mathrm{km\,s^{-1}}$.

At the time of our radio map, the Hα profile of RS Oph has greatly changed, as illustrated by the spectrum for day +34.2 in Fig. 3. At that time, the bulk of the ejecta has been significantly slowed down by the pre-existing RG wind, and the dominant component of the H alpha emission has narrowed and reduced in both peak and total intensity. However, a broad pedestal persists – highlighted by the fitting in Fig. 3 – that originates from the ejecta expelled at the highest inclinations from the equatorial plane, and which suffered from the smallest deceleration thanks to the reduced column density of the RG wind

along that direction. On day +34.2, the broad pedestal was still extending up to $-4200\,\mathrm{km\,s^{-1}}$. Given the similarity of these two values, we assume a linear deceleration with time, leading to $v_{\rm eje}\cos i = 4450\,\mathrm{km\,s^{-1}}$ as the mean radial velocity of the leading ejecta during the interval from day 0 to +34.3, where i is the orbital inclination (0° face-on, 90° edge-on).

The tangential velocity of the leading edge of the radio lobes in Fig. 1, averaged over the 34.3 days elapsed since the onset of the outburst, is $v_{\rm eje}\sin i \sim 6100\,\mathrm{km\,s^{-1}}$ at the *Gaia* distance to RS Oph. By comparing with the results from radial velocities, we derive $v_{\rm eje} = 7550(\pm150)\,\mathrm{km\,s^{-1}}$ for the space velocity of the ejecta, and $i = 54°(\pm1)$ for the orbital inclination.

It is interesting to compare the angular extent of the ejecta on our radio map and on the [OIII] 5007 HST imaging of the 2006 ejecta presented by Ribeiro et al. (2009). By day +155, the ejecta had travelled a total east–west extension of 360 ± 30 mas on HST images, which corresponds to $v_{\rm eje}\sin i \sim 5400(\pm500)\,\mathrm{km\,s^{-1}}$ at the *Gaia* distance. This is very close to our $v_{\rm eje}\sin i \sim 6100\,\mathrm{km\,s^{-1}}$ estimated from the radio imaging in Fig. 1, especially considering that (a) some further deceleration may have occurred between days +34.3 and +155, and (b) [OIII] 5007 forms as a consequence of ion recombination, which is favoured by a larger electron density, which is easier to encounter at inner radii of the ejecta in homologous expansion compared to the radio synchrotron emission originating at their outer edge. It may then be concluded that the ejection velocity in both 2006 and 2021 eruptions was very similar, and that the orbital phase (the RG transiting at the ascending quadrature in 2006 and at the descending one in 2021) made no difference.

At about day +22/+23 into the outburst, permitted lines began showing a triple-peaked profile that progressively grew in contrast relative to the much wider, underlying broad component. HeI 6678 on the day +34.2 spectrum of Fig. 3 shows an example of such a profile (for Balmer lines, it only became visible at much later epochs when their strong broad component weakened considerably). The time of appearance of the triple-peaked profile broadly coincides with the emergence of supersoft X-ray emission (Page et al. 2022), indicating that the triple-peaked profile originates from the inner regions of RS Oph, which became visible only after the ejecta had become sufficiently diluted to clear the view to the central binary. The radial velocity of the outer peaks declined from $\sim250\,\mathrm{km\,s^{-1}}$ at appearance to $\sim150\,\mathrm{km\,s^{-1}}$ by day +102 when RS Oph entered the solar conjunction (Munari & Valisa 2022).

We believe that the outer peaks of the triple-peaked profiles originate from the same location as the CC source in Fig. 1; that is, from the ring where the nova ejecta impact the DEOP and are more severely decelerated by its greater density than by the diffuse RG wind at higher latitudes. Such a high-density location is also supported by the fact that – contrary to permitted lines – the forbidden nebular lines did not develop a tripled peak profile (at least all those characterised by low critical densities for collisional de-excitation, such as the usual [OIII] or [NII]). Assuming that the projected expansion velocity of the CC ring declines exponentially from an initial $6100\,\mathrm{km\,s^{-1}}$ to $250\,\mathrm{km\,s^{-1}}$ on day +22 and $150\,\mathrm{km\,s^{-1}}$ on day +102, by day +34.3 of our EVN image the ring has expanded to a diameter of 11 mas (14.5 AU), which is compatible with the unresolved appearance of the CC in Fig. 1.

Finally, the central peak of the triple-peaked profiles remained relatively sharp (FWHM $\sim 55\,\mathrm{km\,s^{-1}}$) and its radial velocity stayed close to the barycentric velocity of the central binary, suggesting that it may have formed on the side of the RG irradiated by the still burning WD.

4. Conclusions

We present EVN radio imaging at 5 GHz of the expanding ejecta of the recurrent nova RS Oph for day +34 of its 2021 outburst, extending for about 90 mas along the east–west direction. Comparison with *Gaia* DR3 astrometry, radial velocity information from high-resolution optical spectra, and similar radio observations of the 2006 eruption allows us to combine all the observed features into a consistent 3D model. The presence of a strong density enhancement on the orbital plane – seen at $i = 54°$ inclination – confined the nova ejecta primarily into two lobes, expanding in opposite directions perpendicular to the plane at $v_{\rm eje} = 7550\,\mathrm{km\,s^{-1}}$ space velocity, averaged over the first 34 days. The density enhancement partially obscures the receding lobe in the background, and its inner radius impacted by the ejecta is the location of the unresolved and bright central radio spike.

Acknowledgements. We acknowledge the rapid and constructive report by the referee (Stewart Eyres). Scientific results from data presented in this publication are derived from the following EVN project code: RG012E. The European VLBI Network is a joint facility of independent European, African, Asian, and North American radio astronomy institutes. *e*-MERLIN is a National Facility operated by the University of Manchester at Jodrell Bank Observatory on behalf of STFC, part of UK Research and Innovation. BM acknowledges financial support from the State Agency for Research of the Spanish Ministry of Science and Innovation under grant PID2019-105510GB-C31 and through the Unit of Excellence María de Maeztu 2020–2023 award to the Institute of Cosmos Sciences (CEX2019-000918-M). This work has made use of data from the European Space Agency (ESA) mission *Gaia* (`https://www.cosmos.esa.int/gaia`), processed by the *Gaia* Data Processing and Analysis Consortium (DPAC, `https://www.cosmos.esa.int/web/gaia/dpac/consortium`). Funding for the DPAC has been provided by national institutions, in particular the institutions participating in the *Gaia* Multilateral Agreement.

References

Acciari, V. A., Ansoldi, S., Antonelli, L. A., et al. 2022, Nat. Astron., 6, 689
Adamakis, S., Eyres, S. P. S., Sarkar, A., & Walsh, R. W. 2011, MNRAS, 414, 2195
Aydi, E., Chomiuk, L., Izzo, L., et al. 2020, ApJ, 905, 62
Booth, R. A., Mohamed, S., & Podsiadlowski, P. 2016, MNRAS, 457, 822
Brandi, E., Quiroga, C., Mikołajewska, J., Ferrer, O. E., & García, L. G. 2009, A&A, 497, 815
Cheung, C. C., Johnson, T. J., Jean, P., et al. 2022, ApJ, 935, 44
Chomiuk, L., Linford, J. D., Aydi, E., et al. 2021a, ApJS, 257, 49
Chomiuk, L., Metzger, B. D., & Shen, K. J. 2021b, ARA&A, 59, 391
Dobrzycka, D., Kenyon, S. J., Proga, D., Mikolajewska, J., & Wade, R. A. 1996, AJ, 111, 2090
Fekel, F. C., Joyce, R. R., Hinkle, K. H., & Skrutskie, M. F. 2000, AJ, 119, 1375
Gaia Collaboration 2022, VizieR Online Data Catalog: I/355
H.E.S.S. Collaboration (Aharonian, F., et al.) 2022, Science, 376, 77
Keimpema, A., Kettenis, M. M., Pogrebenko, S. V., et al. 2015, Exp. Astron., 39, 259
Lee, Y.-M., Kim, H., & Lee, H.-W. 2022, ApJ, 931, 142
Martin, P., & Dubus, G. 2013, A&A, 551, A37
Munari, U. 2019, Cambridge Astrophys. Ser., 54, 77
Munari, U., & Valisa, P. 2021, ArXiv e-prints [arXiv:2109.01101]
Munari, U., & Valisa, P. 2022, ArXiv e-prints [arXiv:2203.01378]
Nayana, A. J., Anupama, G. C., Banerjee, D., et al. 2021, ATel, 14899, 1
O'Brien, T. J., Bode, M. F., Porcas, R. W., et al. 2006, Nature, 442, 279
O'Brien, T. J., Beswick, R. J., Bode, M. F., et al. 2008, in RS Ophiuchi (2006) and the Recurrent Nova Phenomenon, ASP Conf. Ser., 401, 239
Orlando, S., & Drake, J. J. 2012, MNRAS, 419, 2329
Page, K. L., Beardmore, A. P., Osborne, J. P., et al. 2022, MNRAS, 514, 1557
Pan, K.-C., Ricker, P. M., & Taam, R. E. 2015, ApJ, 806, 27
Peters, W. M., Clarke, T. E., Giacintucci, S., Kassim, N. E., & Polisensky, E. 2021, ATel, 14908, 1
Ribeiro, V. A. R. M., Bode, M. F., Darnley, M. J., et al. 2009, ApJ, 703, 1955
Rupen, M. P., Mioduszewski, A. J., & Sokoloski, J. L. 2008, ApJ, 688, 559
Sokoloski, J. L., Rupen, M. P., & Mioduszewski, A. J. 2008, ApJ, 685, L137
Sokolovsky, K., Aydi, E., Chomiuk, L., et al. 2021, ATel, 14886, 1
Walder, R., Folini, D., & Shore, S. N. 2008, A&A, 484, L9
Williams, D., O'Brien, T., Woudt, P., et al. 2021, ATel, 14849, 1